Available online at www.sciencedirect.com

ScienceDirect

Procedia Structural Integrity 12 (2018) 416–428

Structural Integrity Procedia

www.elsevier.com/locate/procedia

AIAS 2018 International Conference on Stress Analysis

Automatic shape optimization of structural components with manufacturing constraints

Stefano Porziani[a,*], Corrado Groth[a], Marco Evangelos Biancolini[a]

[a]*University of Rome "Tor Vergata", Rome 00133, Italy*

Abstract

Among optimization procedures, mesh morphing gained a relevant position: it proved to be a suitable tool in obtaining weight and stress concentration reduction, without the need to iterate the numerical model generation. Shape modification through mesh morphing can be performed in an automatic fashion adopting two approaches: defining parameters which will describe the modified shape or exploiting results coming from numerical analyses. With this second approach, it is possible to achieve a very high automation grade: stress values retrieved on component surfaces can be successfully employed to drive the shape modification of the component itself. This 'driven-by-numerical-results' automatic approach can lead to complex optimized shapes, which can be easily achieved with modern additive manufacturing processes, but not adopting traditional manufacturing processes. In the present work a method to include manufacturing constraints in a shape optimization workflow is presented and applied to different structural optimization cases, in order to demonstrate how even manufacturing based on traditional processes can take advantage of automatic shape optimization of structural components.

Keywords: FEM; Optimization; Mesh Morphing; Biological Growth Method

1. Introduction

Optimization in mechanical application is a natural paramount for every designer: through optimization it is possible to minimize both costs and failure risks of mechanical components. When dealing with complex component shapes together with complex loads and constraints configurations, the optimization task can become very challenging. The introduction and widespread adoption of numerical simulation in mechanical design furnished valid tools to the designer in charge of optimizing mechanical components: different shapes can be virtually tested using Finite Element Method (FEM) and optimization techniques based on evolutive algorithms or metamodels. To perform the optimization procedure several numerical models are required to be built, which can become a very time-consuming task, specially dealing with complex shape models.

* Corresponding author. Tel.: +39 06 72597136.
E-mail address: porziani@ing.uniroma2.it

2452-3216
10.1016/j.prostr.2018.11.076

A valuable alternative to the rebuilding of the model for each shape (including both the geometrical description of the component and the model remeshing) is the mesh morphing. Mesh morphing (de Boer et Al. (2007), Biancolini (2011) and Staten et Al. (2011)) is a powerful tool that allows to generate different model shapes by only modifying the mesh nodes position, without the need of remeshing. This technique proved its reliability in several engineering fields. Biancolini and Groth (2014) successfully applied mesh morphing in simulating ice accretion on aircraft wings in Computational Fluid-Dynamics (CFD) simulations. Biancolini and Cella (2010) used mesh morphing to study the coupling of CFD and Computational Structural Mechanics (CSM) in an aeroelastic application. Cella et Al. (2017) adopted mesh morphing in geometric parametrization for shape optimization. Biancolini et Al. (2018) exploited mesh morphing in the study of crack shapes, including the proposal of an automatic procedure to simulate the crack propagation. An interesting approach in automatic optimization was illustrated by Groth et Al. (2018), which coupled an adjoint solver with mesh morphing in a gradient based optimization obtaining a high computational and optimization efficiency. This approach exploits information from the adjoint solver on model surfaces to decide where and how to sculpt the surface itself in order to pursuit a specific goal (i.e. stress optimization).

Another approach that uses surface stress information to decide where apply a modification is the Biological Growth Method, which is based on biological tissue under stress behaviour (see section 1.2). Although this method can be successfully employed to optimize mechanical component shape, it could generate complex surfaces that can hardly be realized if the manufacturing processes are subjected to specific manufacturing constraints.

In the present work a methodology to overcome these limits is be presented: in the framework of ANSYS® Workbench™ Finite Element Analysis (FEA) tool, the Radial Basis Functions (RBFs) based mesh morpher tool RBF Morph, was used to generate optimized shapes consistent with linear and circular manufacturing constraints. This goal was achieved exploiting the coordinate filtering functionality of the mesh morpher tool.

Coordinate filtering complying both linear and circular manufacturing constraint was employed with the parameter-based optimization approach and with the BGM approach, so that a final morphed shape suitable for traditional manufacturing processes can be obtained adopting both optimization approaches.

1.1. RBF Background

RBFs are a class of mathematical functions introduced in the early 60s as an interpolation method for multidimensional scattered data (Davies (1963)). The main advantage of such mathematical tool is that it is possible to interpolate everywhere in the space a scalar function defined at discrete points, called source points, obtaining the exact value of the scalar function evaluated at source points. If the data to be interpolated is given in the form of scattered scalar values at a series of source point $\boldsymbol{x}_{k_i}$ in the space $\mathbb{R}^n$, the interpolating function in the same space can be evaluated at a generic location $\boldsymbol{x}$ as presented in (1).

$$s(\boldsymbol{x}) = \sum_{i=0}^{N} \gamma_i \varphi \left(\left\| \boldsymbol{x} - \boldsymbol{x}_{k_i} \right\| \right) \tag{1}$$

The points $\boldsymbol{x}$ at which the function is evaluated are the target points. φ is the so-called radial basis function, which is a scalar function of the Euclidean distance between each source point and the target point considered. γ_i are the weights of the radial basis which are to be evaluated solving a linear system of equations, whose order is equal to the number of source points introduced. The behavior of the function in the space between the source points depend on the RBF type adopted; typical RBF are shown in Table 1, considering $r = \left(\left\| \boldsymbol{x} - \boldsymbol{x}_{k_i} \right\| \right)$.

To guarantee the existence and the uniqueness of the solution a polynomial part h is added to the interpolation function presented in (1) .

$$s(\boldsymbol{x}) = \sum_{i=1}^{N} \gamma_i \varphi \left(\left\| \boldsymbol{x} - \boldsymbol{x}_{k_i} \right\| \right) + h(\boldsymbol{x}) \tag{2}$$

Table 1. Most common RBFs.

RBF type	Equation
Spline type (Rn)	$r^n,\ n\ odd$
Thin plate spline	$r^n log(r),\ n\ even$
Multiquadric (MQ)	$\sqrt{1+r^2}$
Inverse multiquadric (IMQ)	$\frac{1}{\sqrt{1+r^2}}$
Inverse quadric (IQ)	$\frac{1}{1+r^2}$
Gaussian (GS)	e^{-r^2}

The degree of polynomial h depends on the RBF type adopted for the interpolation problem. The weights γ_i and the coefficient of the polynomial can be found if the following conditions are satisfied:

$$\begin{aligned} s(\boldsymbol{x}_{k_i}) &= g_i \\ h(\boldsymbol{x}_{k_i}) &= 0 \end{aligned} \qquad 1 \leq i \leq N \tag{3}$$

In (3) g_i are the given values at source points $\boldsymbol{x}_{k_i}$. A condition of orthogonality is also required:

$$\sum_{i=1}^{N} \gamma_i p\left(\boldsymbol{x}_{k_i}\right) = 0 \tag{4}$$

for all polynomials p with a degree less or equal than that of polynomial h. A unique interpolator exists if the basis functions is a conditionally positive definite function. If a linear polynomial is chosen in a 3D space

$$h(\boldsymbol{x}) = \beta_1 + \beta_2 x + \beta_3 y + \beta_4 z \tag{5}$$

a non-singular square system can be obtained as follows:

$$\begin{bmatrix} \mathbf{M} & \mathbf{P} \\ \mathbf{P}^T & 0 \end{bmatrix} \begin{pmatrix} \boldsymbol{\gamma} \\ \boldsymbol{\beta} \end{pmatrix} = \begin{pmatrix} \boldsymbol{g} \\ 0 \end{pmatrix} \tag{6}$$

$\mathbf{M}$ is the interpolation matrix

$$\mathbf{M}_{i,j} = \varphi\left(\boldsymbol{x}_{k_i} - \boldsymbol{x}_{k_j}\right) \qquad 1 \leq i, j \leq N \tag{7}$$

$\mathbf{P}$ is a constraint matrix that arises in the system to balance the polynomial contribution and contains a columns of "1" and the coordinates of source points in following columns:

$$\mathbf{P} = \begin{bmatrix} 1 & \boldsymbol{x}_{k_1} & \boldsymbol{y}_{k_1} & \boldsymbol{z}_{k_1} \\ 1 & \boldsymbol{x}_{k_2} & \boldsymbol{y}_{k_2} & \boldsymbol{z}_{k_2} \\ \vdots & \vdots & \vdots & \vdots \\ 1 & \boldsymbol{x}_{k_N} & \boldsymbol{y}_{k_N} & \boldsymbol{z}_{k_N} \end{bmatrix} \tag{8}$$

RBFs can be applied to mesh-morphing: the RBFs are used to evaluate a vector field of displacement, which can be accomplished by interpolating each component as an independent scalar field:

$$\begin{cases} s_x(\boldsymbol{x}) = \sum_{i=0}^{N} \gamma_i^x \varphi\left(\|\boldsymbol{x} - \boldsymbol{x}_i\|\right) + \beta_1^x + \beta_2^x x + \beta_3^x y + \beta_4^x z \\ s_y(\boldsymbol{x}) = \sum_{i=0}^{N} \gamma_i^y \varphi(\|\boldsymbol{x} - \boldsymbol{x}_i\|) + \beta_1^y + \beta_2^y x + \beta_3^y y + \beta_4^y z \\ s_z(\boldsymbol{x}) = \sum_{i=0}^{N} \gamma_i^z \varphi(\|\boldsymbol{x} - \boldsymbol{x}_i\|) + \beta_1^z + \beta_2^z x + \beta_3^z y + \beta_4^z z \end{cases} \tag{9}$$

The source points of the RBF fit problem are the nodes that have to be moved according to a prescribed displacement. The morphing action can be limited to the desired zones of the mesh by imposing a zero displacement to those nodes that wrap the interested area. It is worth to remark that the mesh-morphing can affect the mesh quality and the success of the morphing action depends on the skill of the user.

1.2. BGM Method

The Biological Growth Method (BGM) is a shape optimization method focused on stress of structural parts. This method is based on the observation that biological structures as tree trunks and animal bones evolve by adding new layers of biological material at surface with a stress promoted growth rate. Heywood (1969) and Mattheck et Burkhardt (1990) proposed to extend this concept: material can be added on surfaces with high stresses and can be removed from surfaces where stresses are low. Heywood (1969) demonstrated that, thanks to photoelastic techniques it is possible to obtain a uniform stress along the boundary of a stress concentrator by tuning the boundary itself according to BGM approach. Mattheck et Burkhardt (1990) presented a 2D study capable to predict the shape evolution observed in natural structures and proposed this approach to be used in CAE based optimization, presenting also the result obtained with a plate with a circular hole and with a chain link. In their work, the authors computed the volumetric growth ($\dot{\varepsilon}$) according to the von Mises stress (σ_{Mises}) and a threshold stress (σ_{ref}); the latter one was chosen according to the allowable stress for the specific design.

$$\dot{\varepsilon} = k\left(\sigma_{Mises} - \sigma_{ref}\right) \tag{10}$$

Waldman and Heller (2015) proposed a more refined model for layer growth, suitable for shape optimization of holes in airframe structures with multiple stress peak locations. The formula is more complex than (10), as reported in (11):

$$d_i^j = \left(\frac{\sigma_i^j - \sigma_i^{th}}{\sigma_i^{th}} \right) \cdot s \cdot c \,, \qquad \sigma_i^{th} = max(\sigma_i^j) \text{ if } \sigma_i^j > 0 \quad \text{or} \quad \sigma_i^{th} = min(\sigma_i^j) \text{ if } \sigma_i^j < 0 \tag{11}$$

The model by Waldman and Heller moves the i-th boundary node of the j-th region by a distance d_i^j, computed using (11), where σ_i^j is the tangential stress, σ_i^{th} is the stress threshold, c is and arbitrary characteristic length and s is a step size scaling factor.

In the present work a different implementation of BGM is used. As stated before, the framework used to perform numerical simulations is ANSYS® Mechanical™ exploiting the RBF Morph ACT Extension. The capability of RBF Morph in performing BGM optimization were already presented in Biancolini (2018). The BGM implemented is define the node displacement (S_{node}) in the direction normal to the surface according to (12), where σ_{node} is the stress evaluated at each node, σ_{th} is a threshold value for stress defined by user, σ_{max} and σ_{min} are respectively the maximum and the minimum value of stress in the current set. d is the maximum offset between the nodes on which the maximum and the minimum stress are evaluated; this parameter is defined by the user to control the nodes displacement whilst limiting the possible distortion of the mesh.

$$S_{node} = \frac{\sigma_{node} - \sigma_{th}}{\sigma_{max} - \sigma_{min}} \cdot d \tag{12}$$

As can be easily understood, according to equation (12), nodes on the surface to be optimized can be moved either inward, if the stress on node is lower than the threshold value, or outward, if the evaluated stress is higher than the threshold value. In RBF Morph BGM implementation is possible to perform the optimization according to different equivalent stresses and strains, as summarized in Table 2.

Table 2. Stress and strain types available in the RBF Morph implementation of BGM.

Stress/Strain type	Equation
von Mises stress	$\sigma_e = \sqrt{(\sigma_1 - \sigma_2)^2 + (\sigma_2 - \sigma_3)^2 + (\sigma_3 - \sigma_1)^2}$
Maximum Principal stress	$\sigma_e = max(\sigma_1, \sigma_2, \sigma_3)$
Minumum Principal stress	$\sigma_e = min(\sigma_1, \sigma_2, \sigma_3)$
Stress intensity	$\sigma_e = max(\lvert\sigma_1 - \sigma_2\rvert, \lvert\sigma_2 - \sigma_3\rvert, \lvert\sigma_3 - \sigma_1\rvert)$
Maximum Shear stress	$\sigma_e = 0.5 \cdot (max(\sigma_1, \sigma_2, \sigma_3) - min(\sigma_1, \sigma_2, \sigma_3))$
Equivalent Plastic strain	$\varepsilon_e = [2(1+\nu')]^{-1} \cdot \left(0.5\sqrt{(\varepsilon_1 - \varepsilon_2)^2 + (\varepsilon_2 - \varepsilon_3)^2 + (\varepsilon_3 - \varepsilon_1)^2}\right)$

On a generic surface of a mechanical component, the stress distribution can be very complex: in the next sections two different applications are described and analysed in order to demonstrate how the irregular stress distribution can still be used to optimize mechanical components that exhibit linear or circular symmetry exploiting manufacturing constraints.

2. Applications Description

The mechanical components described hereinafter were chosen with the aim of illustrating the developed procedures maintaining as simple as possible the involved geometries. Two applications will be described to illustrate the linear and circular manufacturing constraints of RBF Morph.

Both numerical models described hereinafter are realized using functionalities provided by ANSYS® Mechanical™ FEA tool, in particular material used to model the mechanical components is the standard "Construction Steel" provided in the in the Material Library of the FEA program.

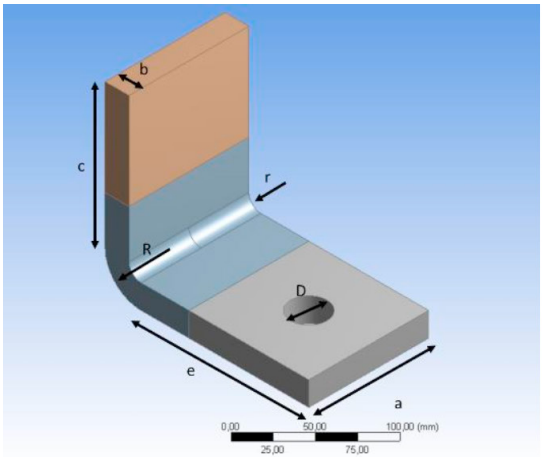

a	100 mm
b	10 mm
c	120 mm
D	30 mm
e	14 0mm
r	10 mm
R	30 mm
a	100 mm

Fig. 1. Bracket geometry and dimensions

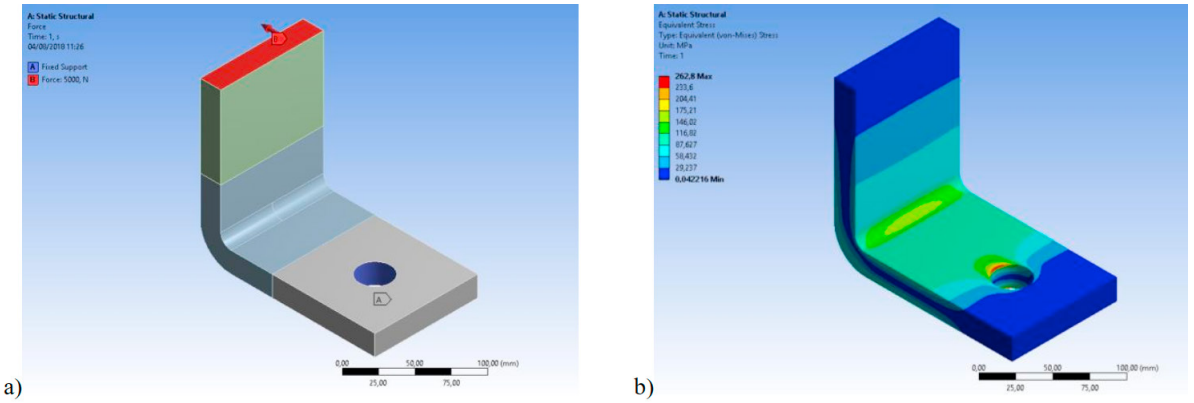

a) b)

Fig. 2. a) Load and constraints; b) von Mises stress distribution

2.1. Bracket linear manufacturing constraints

The first application refers to the optimization of a holed bracket with a fillet (see Fig. 1). The bracket is loaded as reported in Fig. 2a: a fixed constraint is placed on the internal surfaces of the circular hole and a 5000 N load is applied on the upper surface of the vertical plate. As expected, this mechanical component in this specific load and constraint condition has two points in which von Mises stress peaks arise (hot spots, see Fig. 2b): in proximity of the hole and at the centre of the fillet. This latter hot spot will be object of the optimization adopting linear manufacturing constraints, as explained in section 3.

2.2. Pin circular manufacturing constraints

The second application refers to a pin with a circular fillet as depicted in Fig. 3. The lower face of the pin is constrained fixed and a remote force is applied on the upper circular face with a 5000 N force acting in the positive X direction.

Also in this case, the hot spot for von Mises stress is located on the fillet (see Fig. 4); the morphing action will therefore focus on this area in order to optimize the stress peak adopting both BGM and parameter-based optimization.

In the next sections the morphing strategies and the optimization results are illustrated.

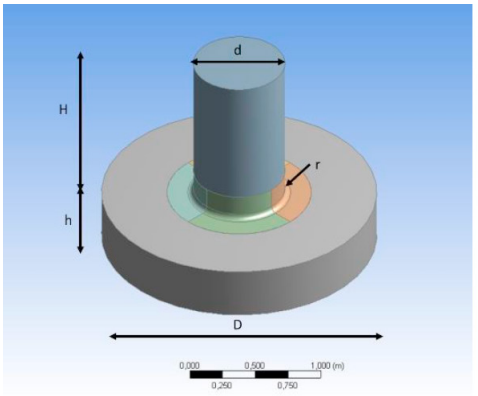

d	700 mm
D	2100 mm
h	400 mm
H	1200 mm
r	210 mm

Fig. 3. Pin geometry and dimensions

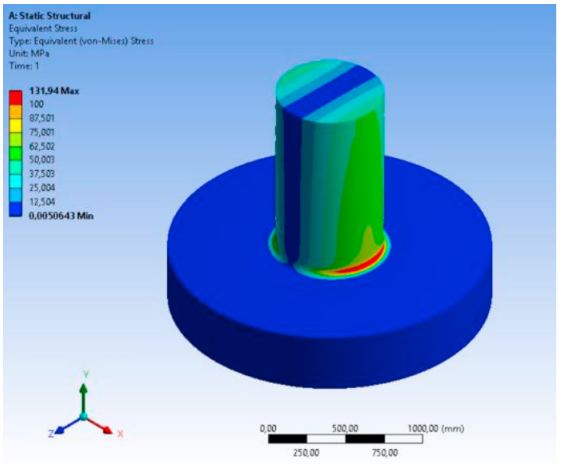

Fig. 4. von Mises stress distribution on the pin

3. Linear manufacturing constraints optimization

As already stated, the optimization of the bracket was performed adopting two strategies: parameter-based and BGM. The first one was carried out taking advantage of the ANSYS® DesignXplorer™ functionalities, in particular the Response Surface Optimization. The morphing action was limited to the central part of the bracket: meshes of the vertical and the horizontal plates were not modified. To generate the optimized shape the profile of the fillet was controlled through three parameters: the two extremal points of the profile tangential displacement and the central point radial displacement (see Fig. 5a). The RBF Morph setup involved the nodes on the surfaces of the interested volume around the fillet: surfaces highlighted in green in Fig. 5b were maintained fixed; furthermore, three translation sets were defined for each of the points reported in Fig. 5a. The shape obtained by moving these three points was then applied to the whole fillet profile using the coordinate filtering capability of RBF Morph. The coordinate filtering allows to sample the shape modification at a selected location (i.e. the section on which the three points are defined) and to replicate it along a specified coordinate direction. According to this setup, the surfaces highlighted in red in Fig. 5b are free to deform.

The parameter-based optimization was performed using as target the minimization of the von Mises stress maximum value on the deformable surfaces and adopting the setup reported in Fig. 6.

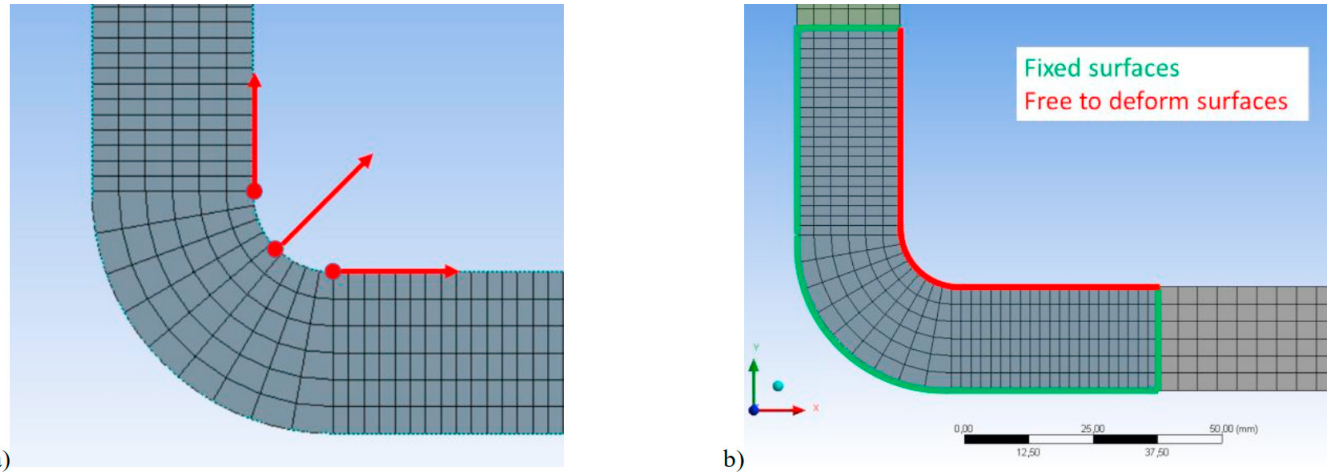

Fig. 5. a) points used to control the fillet shape and their displacement; b) location of fixed and free to deform surfaces

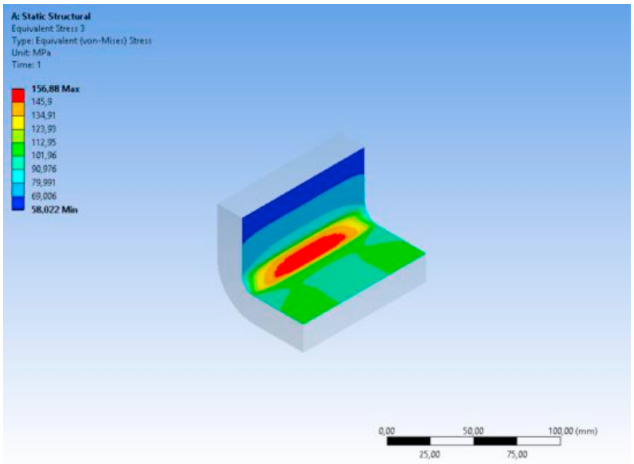

Design of Experiment type	Latin Hypercube
Samples type	CCD Samples
Response Surface type	Kriging
Kernel type	Variable
Refinement points	3 – candidate points

Fig. 6. Bracket deformable surfaces with von Mises stress and response surface optimization setup

After the ANSYS® DesignXplorer™ run, a candidate point was identified: the von Mises stress peak on the internal fillet was reduced to 122 MPa, -21.8% with respect to the initial value of 156 MPa. Stress distribution in this optimized configuration are depicted in Fig.7b and Fig. 7c

The coordinate filtering generated a fillet profile consistent with a linear manufacturing constraint.

When BGM is employed as optimization strategy, resulting shape is more complex than the one observed in Fig. 7a. To comparison purpose only, it is possible to notice the differences between shape in Fig. 7a with shape depicted Fig. 8a and Fig. 8b. This shape is obtained with the BGM without adopting the coordinate filtering and it is clear that such a shape can be hardly obtained with traditional machining (e.g. chip removal).

To overcome these problems, the coordinate filtering of RBF Morph was employed to apply the shape modification according to a linear manufacturing constraint. In this specific case the coordinate filtering was used to sample the shape modification at the fillet hot spot location and then replicated along a specified coordinate direction. In Fig. 9 a comparison between the preview of the BGM prescribed nodes displacements with and without coordinate filtering and with amplified displacement is depicted.

An optimized fillet shape was obtained after performing ten filtered BGM iterations: each iteration foresaw the static solution of the FEM model in the specified load and constraints configuration and the morphing of the fillet surfaces according to the retrieved von Mises stress values on the surface itself. For each cycle the value for σ_{th} and d

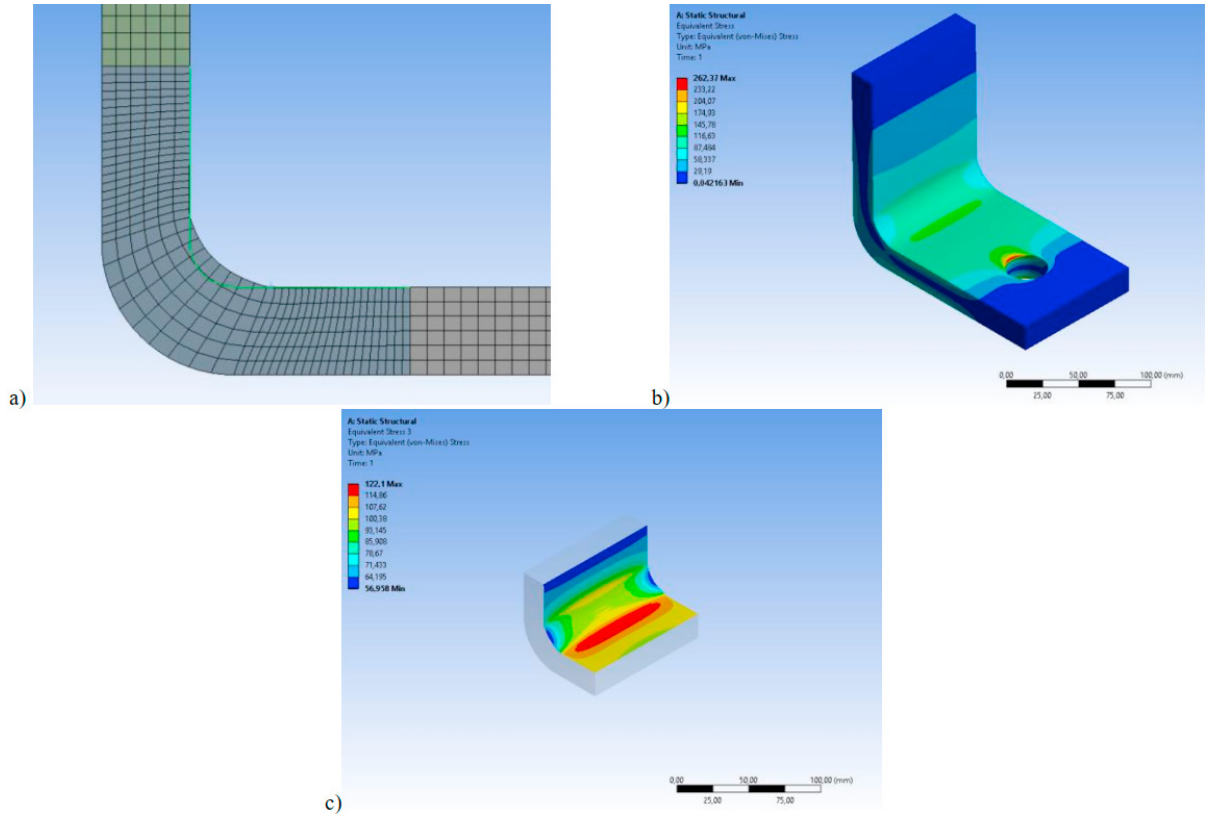

Fig. 7. Bracket parameter-optimized shape: a) mesh; b) von Mises stress distributions on whole component and c) on fillet surface

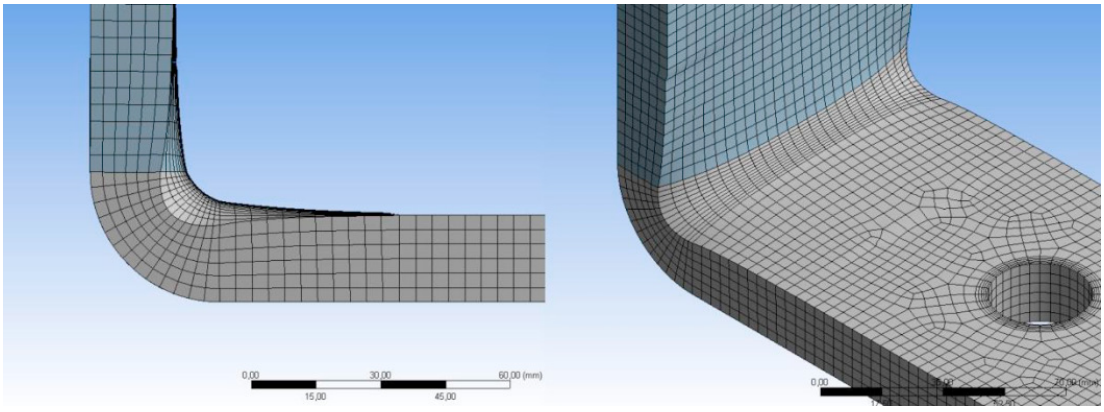

Fig. 8. Optimized configuration obtained with not filtered BGM

of equation (12) were imposed respectively to 100 MPa for von Mises stress and 1 mm. The optimized shape obtained is reported in Fig. 10a whilst von Mises stress distributions on whole component and on the fillet surfaces are depicted respectively in Fig. 10b and Fig. 10c. Maximum von Mises stress value decreased to 108 MPa, -30.7% with respect to the initial value of 156 MPa.

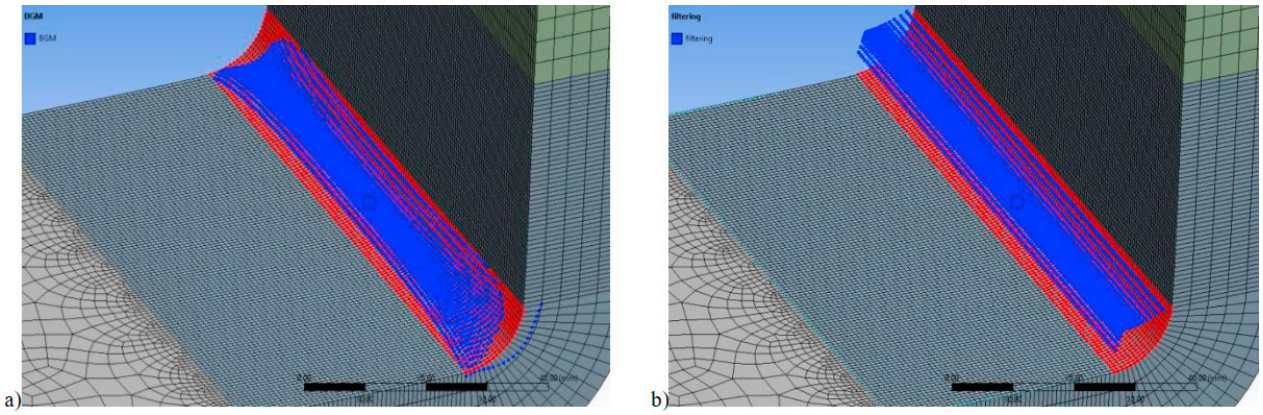

Fig. 9. Preview of nodes displacements: a) with no filtering; b) with filtering amplified displacement

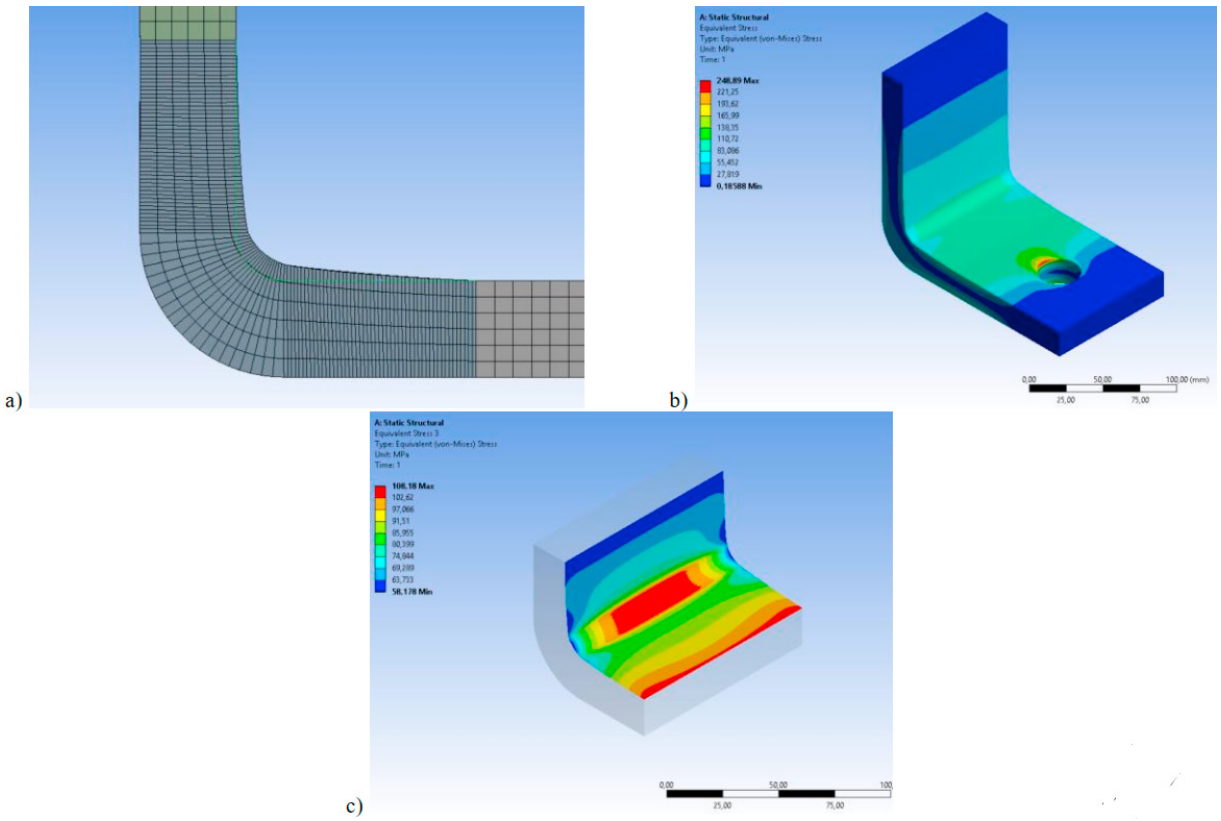

Fig. 10. Bracket BGM-optimized shape: a) mesh; b) von Mises stress distributions on whole component and c) on fillet surface

4. Circular manufacturing constraint optimization

The same approaches described in section 3 were also applied to the component described in section 2.2. The parameter-based optimization was performed imposing the minimization of the maximum von Mises stress value on the surfaces depicted in Fig. 11. To investigate the optimized shape, the same three parameters described in section 3 and represented in Fig. 5a were used to control the fillet profile. In this case, the coordinate filtering used to replicate

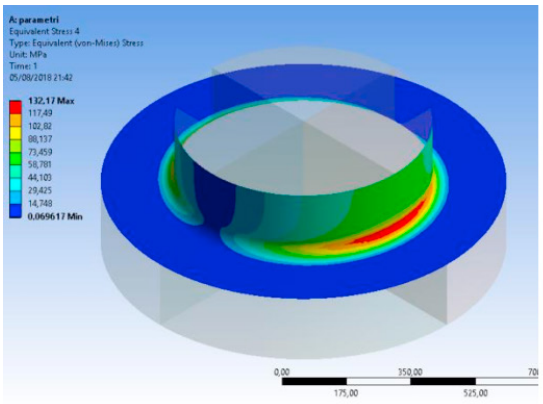

Design of Experiment type	Latin Hypercube
Samples type	CCD Samples
Response Surface type	Kriging
Kernel type	Variable
Refinement points	3 – candidate points

Fig. 11. Pin deformable surfaces with von Mises stress and response surface optimization setup

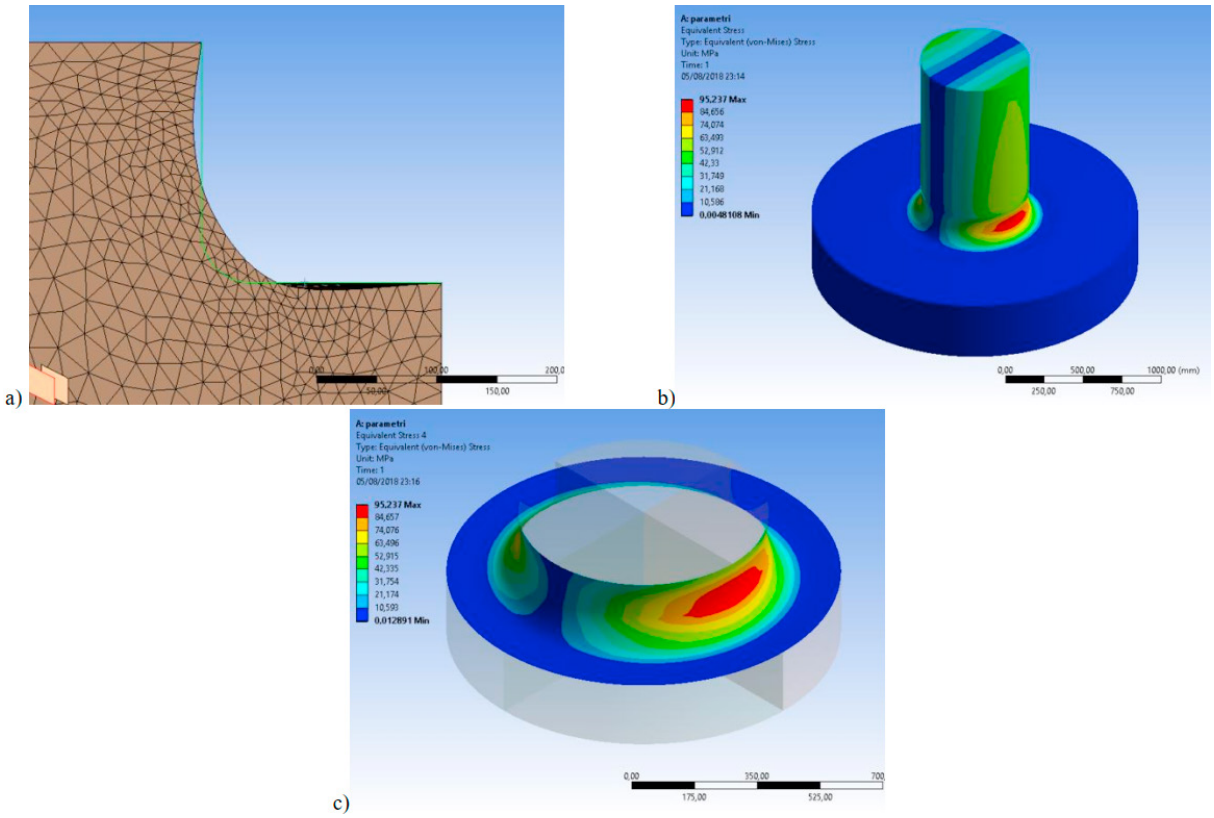

Fig. 12. Pin parameter-optimized shape: a) mesh; b) von Mises stress distributions on whole component and c) on fillet surface

the shape obtained along the whole profile was circular, in order to obtain a modified shape compatible with a circular manufacturing constraint.

The optimized shape identified by ANSYS® DesignXplorer™ is reported in Fig. 12a, whilst the maximum von Mises stress value on the fillet decreased to 95 MPa, -28% with respect to the initial value of 132 MPa. Stress distributions on the whole component and on the fillet surfaces are depicted respectively in Fig. 12b and Fig. 12c

As for the bracket application, an optimization via BGM was also performed. In this case, applying the BGM without the coordinate filtering would have result in an optimized shape without any axial symmetry. Coordinate

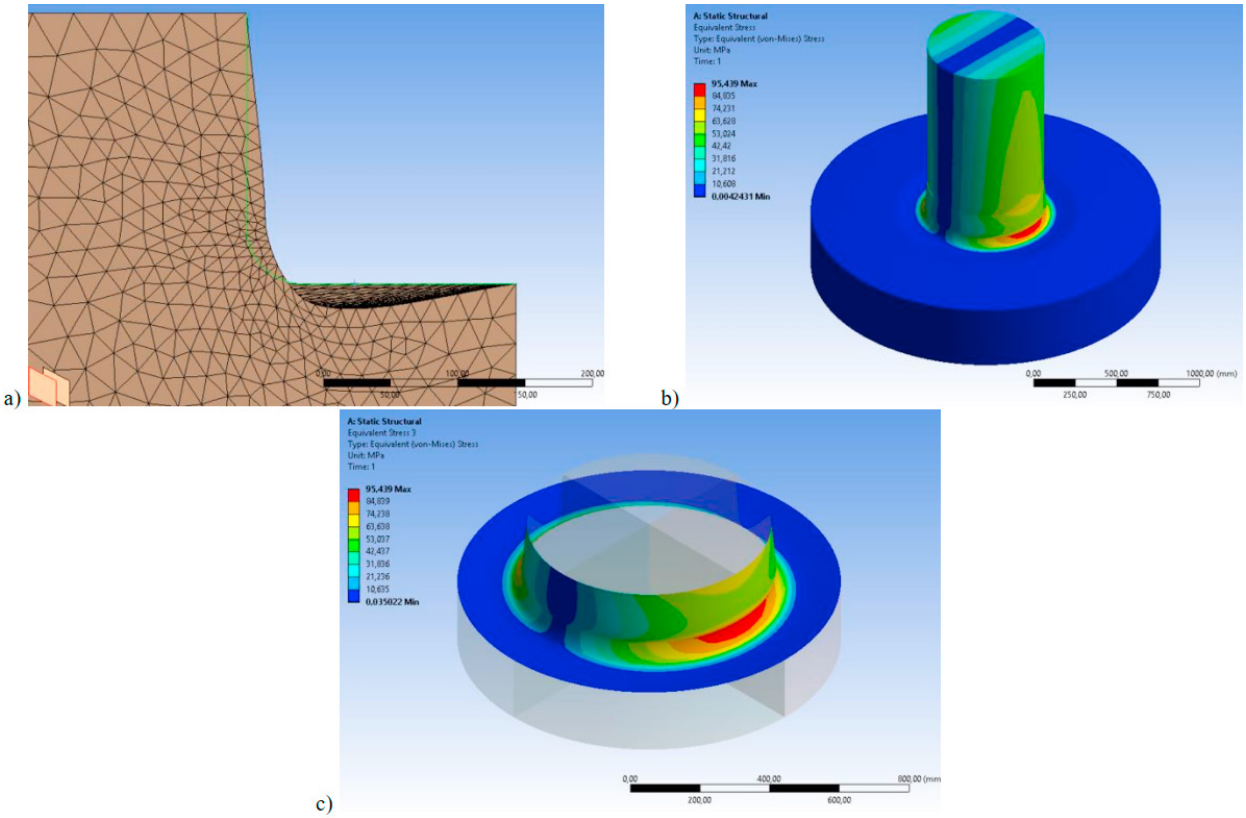

Fig. 13. Pin BGM-optimized shape: a) mesh; b) von Mises stress distributions on whole component and c) on fillet surface

filtering allowed to obtain a final shape compatible with circular manufacturing constraints. The optimized fillet shape was obtained after performing ten filtered BGM cycles sequentially. For each cycle the value for σ_{th} and d were imposed respectively to 75 MPa for von Mises stress and 5 mm. The optimized shape obtained is depicted in Fig. 13a whilst von Mises stress distributions on whole component and on the fillet surfaces are depicted respectively in Fig. 13b and Fig. 13c. Maximum von Mises stress value decreased to 95 MPa, -28% with respect to the initial value of132 MPa.

5. Conclusions

In the present work two optimization strategies were illustrated with the aim of presenting a methodology to generate from them shapes that are suitable for being manufactured with traditional processes. The whole methodology is developed in the ANSYS® Workbench™ environment, in which RBF Morph mesh morphing tool was integrated. The geometries chosen to illustrate the methodology where characterized by linear and circular features and the optimized shape should have kept these characteristics. Generally speaking, the selected optimization strategies does not guarantee that linear or cyclic symmetries are respected. The optimization was carried out both controlling the shapes using three parameters and adopting the BGM approach to optimize the stress levels on the component surfaces. Results from both approaches were filtered in order to obtain final shapes that were consistent with the original component symmetry.

Optimization results of the presented application led in all cases to a substantial decrease of the maximum von Mises stress in the hot spot of interest (stress decreases were in the range of 21% to 30%). The stress decrease levels proved that the proposed methodology can be successfully adopted and implemented in the design cycle of those parts or components that are realized with processes that are subjected to circular and linear manufacturing constraints.

References

Biancolini, M. E., Cella, U., 2010. An advanced RBF Morph application: Coupled CFD-CSM aeroelastic analysis of a full aircraft model and comparison to experimental data, 8th MIRA International Vehicle Aerodynamics Conference. Grove, United Kingdom.

Biancolini, M. E., 2011. Mesh morphing and smoothing by means of radial basis functions (RBF): a practical example using fluent and RBF morph, in "*Handbook of research on computational science and engineering: theory and practice*", 2. IGI Global, Hershey PA, 347−380.

Biancolini, M. E., Groth, C., 2014. An efficient approach to simulating ice accretion on 2D and 3D airfoils. Advanced Aero Concepts, Design and Operations conference. Bristol, United Kingdom.

Biancolini, M. E., Chiappa, A., Giorgetti, F., Porziani, S., Rochette, M., 2018. Radial basis functions mesh morphing for the analysis of cracks propagation. Procedia Structural Integrity 8, 433−443.

Biancolini, M. E., 2018. Fast Radial Basis Functions for Engineering Applications, Springer, Berlin.

Cella U., Groth C., Biancolini M.E., 2017. Geometric Parameterization Strategies for shape Optimization Using RBF Mesh Morphing, in "Advances on Mechanics, Design Engineering and Manufacturing". In: Eynard B., Nigrelli V., Oliveri S., Peris-Fajarnes G., Rizzuti S. (Eds). Springer, Cham. 537−545

Davies P. J., 1963. Interpolation and approximation, Blaisdell, London.

de Boer, A., Van der Schoot, M.S., Bijl, H., 2007. Mesh deformation based on radial basis function interpolation. Computers & structures 85, 784−795.

Groth, C., Chiappa, A., Biancolini, M. E., 2018. Shape optimization using structural adjoint and RBF mesh morphing. Procedia Structural Integrity 8, 379−389.

Heywood R. B., 1969. Photoelasticity for designers, Pergamon Press, Oxford.

Mattheck C., Burkhardt S., 1990. A new method of structural shape optimization based on biological growth. International Journal of Fatigue 12, 185−190.

Staten, M. L., Owen, S. J., Shontz, S. M., Salinger, A. G., Coffey, T. S., 2011. A comparison of mesh morphing methods for 3D shape optimization, 20th international meshing roundtable. Paris, France.

Waldman W., Heller M., 2015. Shape optimization of holes in loaded plates by minimization of multiple stress peaks. Technical Report, Defence Science and Technology Organisation Fisherman Bend, Australia, Aerospace Div, Apr. 2015.